Published in final edited form as:
Anal Chem. 2016 November 15; 88(22): 10876–10883. doi:10.1021/acs.analchem.6b01410.

Automated, Multiplexed Electrical Impedance Spectroscopy Platform for Continuous Monitoring of Microtissue Spheroids

Sebastian C. Bürgel[*], **Laurin Diener**, **Olivier Frey**, **Jin-Young Kim**, **Andreas Hierlemann**
Department of Biosystems Science and Engineering, ETH Zurich, Mattenstrasse 26, Basel 4058, Switzerland

Abstract

Microtissue spheroids in microfluidic devices are increasingly used to establish novel in vitro organ models of the human body. As the spheroids are comparably sizable, it is difficult to monitor larger numbers of them by optical means. Therefore, electrical impedance spectroscopy (EIS) emerges as a viable alternative to probing spheroid properties. Current spheroid EIS systems are, however, not suitable for investigating multiple spheroids in parallel over extended time in an automated fashion. Here we address this issue by presenting an automated, multiplexed EIS (AMEIS) platform for impedance analysis in a microfluidic setting. The system was used to continuously monitor the effect of the anticancer drug fluorouracil (5-FU) on HCT116 cancer spheroids. Simultaneous EIS monitoring of up to 15 spheroids was performed in parallel over 4 days at a temporal resolution of 2 min without any need for pumps. The measurements were continuous in nature, and the setup was kept in a standard incubator under controlled conditions during the measurements. A baseline normalization method to improve robustness and to reduce the influence of slow changes in the medium conductivity on the spheroid EIS readings has been developed and validated by experiments and means of a finite-element model. The same method and platform was then used for online monitoring of cardiac spheroids. The beating frequency of each cardiac spheroid could be read out in a completely automated fashion. The developed system constitutes a promising method for simultaneously evaluating drug impact and/or toxic effects on multiple microtissue spheroids.

[*]**Corresponding Author**: sebastian.buergel@bsse.ethz.ch.

Notes
The authors declare no competing financial interest.

Europe PMC Funders Author Manuscripts

Europe PMC Funders Author Manuscripts

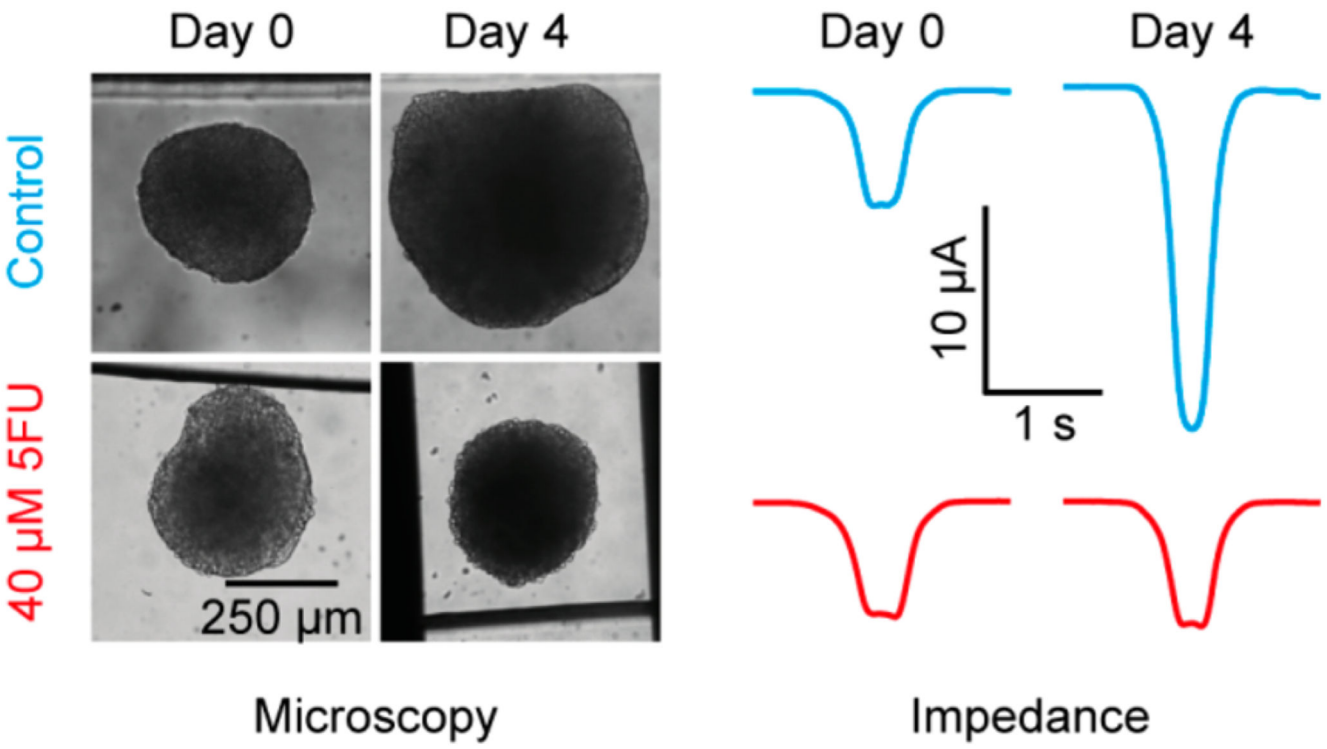

Three-dimensional (3D) microtissue spheroids are emerging as a novel tool for better predicting drug effects, since they more closely mimic an in vivo environment as opposed to conventional two-dimensional cell layers.[1–3] Flat cell cultures cannot sufficiently mimic the cell-to-cell or cell-extracellular matrix interactions found in in vivo systems, and the cells often lose fundamental properties when taken out of their natural environment.[4] Spheroids can be reproducibly fabricated, and different types of spheroids can be handled and used with existing industrial liquid handling systems. The combination of 3D organotypic microtissues with microfluidic devices holds great potential for developing novel in vitro methods for drug screening and toxicology assays. The fluidic interconnection of several different organotypic microtissues on a chip gave rise to developments toward body-on-a-chip platforms.[5–7]

The 3D spheroid systems, however, require new readout techniques, as common readout assays for 2D cell cultures are largely incompatible with the 3D systems. Spheroids with typical diameters of at least 200 μm are difficult to analyze optically in their entirety, even with confocal microscopy, due to the large number of cells and overall volume. Further, advanced imaging methods that feature a large field of view and a large depth of focus in order to assess an entire spheroid are typically not scalable for parallel in situ analysis of many spheroids. Ideally, the new readout methods should not interfere with the experiment and should be continuously applicable in an incubator environment on many samples in parallel in an automated fashion. The beating rates of cardiac spheroids are, for example, very sensitive to temperature changes so that any transfer for analysis will produce artifacts.[8]

Electrical impedance spectroscopy (EIS) receives growing interest as an alternative method to probe the properties of spheroids.[9,10] EIS for spheroid analysis is based on applying an ac voltage to a set of microelectrodes and reading out the resulting current to calculate the corresponding interelectrode impedance values. The characteristic impedance of the microtissue can be measured and analyzed by placing the spheroid between the electrodes. EIS has been previously used, e.g., for the analysis of bacteria,[11] microparticles,[12] single yeast cells,[13] and various blood cell types.[14]

Different systems have been presented to date for EIS analysis of spheroids. Apoptosis or tissue necrosis in breast carcinoma spheroids upon drug exposure has been analyzed by using a capillary screening system.[13] Next, a chip featuring microwells with electrodes located at the side walls for EIS measurements has been used.[14] Spheroids were sequentially loaded into and removed from the measurement cavity by means of a micromanipulator and analyzed at selected time points. Another spheroid EIS chip relied on high-aspect-ratio SU-8 structures within a poly(dimethylsiloxane) (PDMS) channel to trap a spheroid between a set of facing and interdigitated electrodes.[15] It was shown that the EIS measurements could be used to discriminate different dilutions of medium and various spheroid sizes.

The EIS platforms for spheroids mentioned above have a number of limitations for drug testing or toxicity assays. Typically, drug candidates have to be studied on longer time scales (several days), and different compounds have to be analyzed in parallel. Therefore, a system is required which enables (i) continuous recordings over several days, (ii) parallelized readout of multiple tissues, cultured under different conditions, and (iii) automated operation without the need of operator interference with the setup to perform measurements.

Here, we present an automated multiplexed EIS (AMEIS) prototype platform, which is meeting the three requirements outlined above. The integrated platform is targeted at culturing and performing EIS measurements of multiple microtissue spheroids. The device can autonomously acquire impedance spectra of up to 15 individual spheroids over multiple days without the need for interfering with the setup. While the current system has been demonstrated for 15 microtissues in parallel, the architecture and operation of the microsystem, the readout electronics, and the controlling and analysis software were designed to be scalable.

Furthermore, beating cardiac spheroids are particularly sensitive to environmental changes, as, for example, removing them from an incubator for microscopic evaluation can induce temperature changes, which then significantly influence the beating rate.[8] Microscopic evaluation would significantly limit throughput, as the extraction of the beating rate requires video recordings of several seconds per spheroid, a procedure that is typically not suitable for parallelization. Therefore, providing an automated, noninvasive, and label-free in situ assessment method for multiple cardiac spheroids in parallel, which is compatible with a conventional incubator environment, is desirable.

Europe PMC Funders Author Manuscripts

Materials and Methods

Setup

The EIS recordings were conducted during multiple days and, therefore, had to be carried out in a standard incubator environment at 37 °C, 5% CO_2, and 95% relative humidity. As schematically shown in Figure 1A, the chip and the supporting printed circuit board (PCB, AMEIS switch board) were placed in an omni-tray and affixed on a tilting stage. The chip fabrication was based on standard soft lithography and Pt microelectrodes patterning by lift-off as outlined in the Supporting Information. The AMEIS switch board, shown in Figure 1B, multiplexed the analog EIS input/output to any of the 15 chambers and automatically switched from one chamber to another. It featured multiple integrated circuits (IC) for switching, an edge-card connector for electrical interfacing and easy exchange of microfluidic chips, a flat-ribbon connector to the controller board outside the incubator, as well as the two analog SMA connectors connecting to the impedance spectroscope input and output via shielded coaxial cables (see Supporting Information Figure 2 for a view of the PCB back side). The AMEIS switch board was placed inside a standard omni-tray and closed with an environmental lid (LLS-0310, Labcyte Europe, Dublin, Ireland) soaked with PBS. Some modifications were made: access holes for the cables were drilled into the lid and sealed with tape before UV sterilization to minimize the openings of the plate. This approach allowed for maintaining maximal humidity around the chip and limited the evaporation of medium. Impedance measurements were performed with a HF2 impedance spectroscope (Zurich Instruments AG, Zurich, Switzerland) in a frequency range between 10 kHz and 2 MHz; further details can be found in the Supporting Information.

Both the AMEIS switch board and the tilting stage had control units outside the incubator. The connecting cables were fed through a hole in the back wall or through the door of the incubator. The AMEIS controller board outside the incubator was composed of a custom-made PCB and an Arduino (Arduino Uno R3, Arduino LLC, www.arduino.cc) for interfacing to a PC and generating the digital control signals that were required to switch from one spheroid chamber to another. The Arduino software is available at https://github.com/SCBuergel/AMEIS-Arduino (DOI: 10.5281/zeno-do.58204). The Arduino was also keeping track of the currently active spheroid chamber, the identification of which was sent to the impedance spectroscope and recorded along with the EIS data. This procedure simplified subsequent data analysis: it provided the necessary information on which chamber has been recorded at what times. The control software on the PC was a custom C# program, which performed the following four primary tasks: (1) read configurations of the PCB and chip layout, (2) continuous switching through all chambers hosting spheroids in a cyclic fashion, (3) create digital signals for the switch board and tilting controller, and (4) transfer of all these data to the Arduino on the AMEIS controller board. Data were recorded on a PC for later off-line analysis.

Chip Loading

Before use, the chip was sterilized for at least 30 min by UV light in a sterile bench. Afterward, 30 μL of standard medium was introduced into each chamber via the loading ports. Spheroids were prepared as outlined in the Supporting Information and then

individually extracted from the U-bottom 96-well plate by a pipet using a 200 μL tip; all chambers of the chips were filled with one spheroid per chamber through pipetting. During the loading procedure, the chip was manually tilted at least once per minute to prevent any adhesion of the tissues to the channel walls and channel bottom. For control experiments, we used polystyrene beads of 200 and 500 μm diameter (SLGMS-2.5 212-250μm - 10g and PMMAMS-1.2 425-500μm - 5g, Cospheric LLC, Santa Barbara, CA, U.S.A.).

Data Analysis

After the experiment was finished, the recorded data were analyzed by a custom Matlab tool available at https://github.com/SCBuergel/AMEIS-ZI-Matlab (DOI:10.5281/zenodo.58203). The data of all chambers were recorded sequentially and processed in chunks of one chamber at a time. The following steps were performed for each single recording cycle of each chamber: (1) extract baseline current at all simultaneously recorded six frequencies; (2) find peak position using the frequency with the largest baseline current (typically 653 kHz); since the peak is w-shaped, the smaller of the two minima has been used to gain reproducible values over multiple tilting cycles; (3) extract peak-to-baseline currents (ΔI) at all six frequencies using the previously obtained peak position; (4) calculate normalized peak-to-baseline current values (ΔI_{norm}) by dividing the ΔI value by the corresponding baseline value; (5) calculate the start-point-normalized peak-to-baseline current values ($\Delta I_{\mathrm{norm,0}}$) by dividing the ΔI_{norm} values by the start value ΔI_{norm} (t = 0); (6) store baseline, ΔI, ΔI_{norm}, $\Delta I_{\mathrm{norm,0}}$ for each of the six frequencies along with timestamp and chamber index for plotting of spectra or data sequences over multiple days.

Results and Discussion

Time-Domain Analysis

The platform presented in Figure 1 was designed to record EIS data of multiple spheroids over extended periods of time. The spheroid cultivation and measurement relied on periodically tilting the entire platform at defined times. Tilting induced a difference in hydrostatic pressures between the two connected medium reservoirs (cf. Figure 1E). The medium was consequently flowing from the higher-level reservoir through the channel containing the spheroid into the lower-level reservoir. The spheroid was moved over the electrode set to the lower end of the microchannel by gravity and liquid drag forces of the medium flow. Repeated back-and-forth tilting of the platform served three goals: (1) medium perfusion of the spheroid without use of tubings and pumps, (2) prevention of adhesion of the spheroid to the channel surfaces without any need for surface treatment, and (3) back-and-forth shuttling of the spheroid over the set of EIS measurement electrodes at defined times to perform dynamic round-robin EIS recordings.

Tilting the platform and switching the EIS recording from one chamber to another was achieved via an Arduino-based AMEIS controller board in an automated fashion: as schematically shown in Figure 2A, the stage, which holds the microchip,was tilted in periodic intervals (top row). The tilting caused a movement of the spheroid over the electrodes, which yielded a characteristic spike in the current (bottom row). EIS recordings were interrupted, while the AMEIS controller board was sending a switch control signal to

the AMEIS switch board holding the microchip. Upon receiving the entire switch sequence (indicated as SS1, SS2, SS3 in the center row), the EIS signal was recorded from the next chamber. The controller board was then sending a tilt signal (indicated as TS) to the tilting stage controller in order to initiate the next tilting step of the stage. In this way, the single analog input and output of the impedance spectroscope were sequentially multiplexed to each of the 15 chambers in an automated cyclic fashion for multiday EIS recordings.

Whenever a spheroid was passing over the electrode set, it changed the impedance between the two electrodes. To measure the impedance, an impedance spectroscope was used to apply ac voltages of different frequencies and constant amplitudes of 200 mV between a set of coplanar electrodes. The resulting currents were measured via the external transimpedance amplifier. The output voltage of this amplifier was fed back to the impedance spectroscope. The recorded current depicted in Figure 2, parts A and B, as well as the results from finite the finite element model in Supporting Information Figure 5 show a characteristic w-shaped dip, when a spheroid was moving over the electrodes. Since the cell membranes were less conductive than the surrounding medium,[16–18] the presence of the spheroid increased the interelectrode impedance and reduced the recorded current. The level of the baseline before and after the passage of the spheroid depends on the electrical properties of the medium, the electrodes, and interfaces. Peak-to-baseline currents (ΔI, as indicated in Figure 2A) were automatically extracted for every measurement point recorded in every chamber and later analyzed for multiday monitoring (Figure 4). Since parasitics and medium compositions varied from chamber to chamber, the baseline current of each chamber was different, as can be seen in Figure 2B. Switching between chambers every 8 s yielded a temporal resolution of 2 min for a measurement cycle including all 15 chambers. The tilt-and-switch concept thus enabled medium perfusion and shuttling of the spheroid over the EIS electrode set for sequential evaluation of multiple tissues and different electrode sites. Additionally, rolling the spheroid over the electrode pair is advantageous in comparison to immobilizing it on an electrode as this procedure enables a baseline drift compensation as discussed below.

Frequent tilting of the chamber can further be used as a strategy to prevent adhesion of spheroids to the channel walls and channel bottom. In an experiment, shown in Supporting Information Figure 3, the tilting interval of the measurement platform was logarithmically varied from 15 s to 170 min. For tilting intervals below 20 min, all 15 spheroids were moving over the electrodes, yielding an impedance signal as shown in Figure 2B. For increasing tilting intervals beyond 20 min, more and more tissues were adhering to the channel walls. For the largest interval of 170 min only 3 of 15 spheroids (20%) were still moving. Even longer tilting intervals could not be evaluated, as the spheroids started to dissociate. This dissociation was most likely caused by insufficient nutrient supply in the stagnant medium: nutrient diffusion from the reservoir through the microchannel is slow, and the medium volume surrounding the spheroid in the confined microchannel is very limited.

Frequency Domain Analysis

Further insights into the electrical properties of medium and spheroids were gained by multifrequency recordings. The current spectra in Figure 3A were obtained by evaluating the baseline currents as shown in Figure 2 for each of the six recorded frequencies. Thus, the fifth magnitude value from the left (653 kHz) of the baseline spectrum in Figure 3A corresponds to the baseline value of one chamber observed in the time domain in Figure 2. At frequencies below 100 kHz, the magnitude increased with increasing frequencies. This is due to the electric double layer at the electrode-liquid interface, which shows capacitive behavior and, therefore, entails lower impedance—and higher currents—for increasing frequencies. For frequencies larger than 1 MHz, the magnitude decreased due to coupling losses.

Despite using humidifier pads below and above the chip and placing the setup in a maximum-humidity incubator, slight evaporation of medium was observed. This was evidenced in the EIS measurements by increasing baseline currents across the spectrum in Figure 3A over the course of 2 days. Over time, the current increased across all frequencies, since the evaporating water led to an up-concentration of salts. Thus, the conductivity of the medium increased, yielding higher currents between the electrodes. Exchanging the medium after 2 days led to initially decreased currents, which later again increased due to evaporation.

The peak-to-baseline current spectrum in Figure 3B was obtained by subtracting the baseline current from the dip minimum (cf. Figure 2) at each frequency. This spectrum reflects the characteristic properties of the spheroid. The decreasing peak-to-baseline currents (increasing absolute values) over time at all frequencies suggest a growth of the spheroid. An increasing size of a spheroid led to increasing interelectrode impedance and, thus, increasing peak-to-baseline values at all frequencies. Any subsequent single-frequency analysis was carried out at the frequency with the highest absolute ΔI values of 81 kHz. Growth of the spheroid was monitored optically at selected time points as shown in Figure 3C. The optically observed growth of the spheroid from a diameter of 370 μm (day 0) to 470 μm (day 2) and 590 μm (day 4) confirm the continuously acquired data by EIS.

The importance of dynamic instead of static EIS recordings can be seen in Figure 3, parts A and B: the change in baseline magnitude due to evaporation over time (20 μA over 1 day at 653 kHz, cf. Figure 3A) was significant compared to the changes in the peak-to-baseline magnitudes due to spheroid growth (4 μA over 1 day at 653 kHz, cf. Figure 3B). This was despite all efforts to reduce evaporation including a maximumhumidity incubator and the use of humidifier pads. Precise measurements of slow spheroid growth without monitoring the medium conditions are thus not possible. While monitoring medium properties via a separate set of electrodes is possible, the use of the very same integrated electrode set is preferable, as the interpretation of results is straightforward due to a lower number of parasitic elements and no difference in drift behavior. Decoupling the measurements of medium and spheroid impedance may also enable the dosing of compounds while monitoring their concentration.

Continuous Measurements

The presented platform allows for continuous multiday EIS measurements of up to 15 spheroids. The electrically and fluidically separated chambers (cf. Figure 1D) contained one spheroid each. For every activation of the electrodes and tilting of the platform, the impedance spectrum was simultaneously recorded at multiple frequencies in parallel and with the same electrode set. The impedance measurement time of one chamber was set to 8 s so that one measurement cycle of all 15 chambers took 2 min. This was deemed sufficient, as the time scales of spheroid growth, death, or of physiological changes are typically on the order of hours or days.[19] The 81 kHz peak-to-baseline currents ΔI recorded from one spheroid over 4 days are shown in Figure 4A. As in Figure 3B, the peak-to-baseline currents decreased due to growth of the tissue. Rotation and position differences of the spheroid during the impedance measurements led to slight variations in the peak-to-baseline current values of subsequent measurements, as can be seen looking at the individual data points in Figure 4A.

Baseline Drift Compensation

The medium exchange after 42 h led to a significant kink in the peak-to-baseline current plot in Figure 4A. This can be explained by a slow change in medium conductivity due to evaporation. As evaporation can be quantified by the shift of the baseline (Figure 3A), the data were normalized (divided) by the corresponding baseline current values to yield the normalized peak-to-baseline currents (ΔI_{norm}) in Figure 4B. These normalized ΔI_{norm} data do not show decreasing values or a kink upon medium exchange, since the influence of changes in medium conductivity was eliminated by the normalization. The continuous decrease of the normalized peak-to-baseline signal was observed for all growing cancer spheroids. Exemplary 4 day recordings of six cancer spheroids shown in Figure 4C were smoothed by a moving-average method including 10 subsequent measurement values for better visualization. All cancer spheroids in Figure 4C were growing so that ΔI_{norm} decreased over time. The different growth rates, reflected by different slopes in ΔI_{norm}, can be attributed to differences in initial tissue size and, hence, in the number of growing cells. A control experiment using a nongrowing pancreatic microislet is shown in Figure 4D: ΔI_{norm} did not change significantly over the course of 36 h, which also demonstrates the stability of the setup and measurements. Since microislets are much smaller (~150 μm diameter) than the cancer spheroids used here (300-600 μm diameter), the ΔI_{norm} values in Figure 4D are considerably smaller than those in Figure 4, parts B and C. These measurements show the robustness of the method even for small spheroids, which only cover a fraction of the measurement volume (500 μm × 700 μm × 580 μm). A second control experiment shown in Supporting Information Figure 4 was performed with beads of diameters between 200 and 500 μm. It shows the stability of the signals for measurements over 4 days with relative variations in impedance values of below 10% for all bead sizes. This suggests that slight variations in media salinity due to evaporation do not lead to significant changes in ΔI_{norm}. As previously reported,[13,14] the impedance signals scaled with the size of the beads.

The validity of baseline normalization as a means for decoupling the ΔI_{norm} values from media conductivity was further supported by a finite-element model shown in Supporting Information Figure 5. The model in Supporting Information Figure 5A comprises a 2D

representation of the microchannel with two electrodes at the bottom and a nonconductive spherical particle in the channel. Simulated values for baseline current and peak-to-baseline current were obtained by calculating the current density at the electrode surface for different positions of the spherical particle. The position of the spheroid for the current minimum was obtained by sweeping the spheroid position axially along the channel as shown in Supporting Information Figure 5B. That position was then used to calculate the minimal current between the electrode set. The simulation also showed that the two minima in the measured time-domain current in Figure 2A corresponded to the spheroid passing the regions of the strongest electric field at the inner edges of the electrode set. A second simulation of the current was performed without the spheroid to obtain the baseline current. Peak-to-baseline values (ΔI) were then obtained by subtracting the current density peak value from the baseline value.

For obtaining baseline-normalized peak-to-baseline values (ΔI_{norm}), peak-to-baseline currents were divided by the corresponding baseline currents. Both the ΔI and ΔI_{norm} values were plotted in Supporting Information Figure 5C for a variety of different medium conductivities and two different particle sizes. It can be seen that the ΔI_{norm} values featured negligible dependence on the medium conductivity for conductivity variations between 0.5 and 5 S/m compared to a relative change of approximately 20% upon increasing the particle size from 300 to 350 μm.

Monitoring Drug Response through EIS

The growth of HCT116 cancer spheroids has been assessed in the presence of the anticancer drug 5-FU (fluorouracil). In Figure 4, we show results for one spheroid per condition, and we analyzed the very same spheroid continuously by means of EIS, microscopic imaging at day 0, day 2, and day 4, as well as an end-point ATP assay. In total we used three spheroids per condition, of which usually two spheroids could be assessed over the full period of 4 days. The baseline-normalized values ΔI_{norm} (as shown in Figure 4B) were additionally start-point-normalized to obtain the parameter $\Delta I_{\mathrm{norm,0}}$ shown in Figure 5A. $\Delta I_{\mathrm{norm,0}}$, in contrast to ΔI_{norm}, is not sensitive to slight differences in the initial spheroid size. The start point normalization produces rising curves for spheroid growth, as opposed to the falling curves in Figure 4. $\Delta I_{\mathrm{norm,0}}$ values for over 90 h are displayed in Figure 5A and reflect the growth of the three spheroids under control conditions and upon DMSO and 0.4 μM 5-FU exposure. The spheroid treated with 4 μM 5-FU stops to grow after 40 h and starts to dissociate toward the end of the recording. The spheroid exposed to 40 μM 5-FU does not grow during the first 40 h and starts to dissociate thereafter. The trends observed by means of EIS—growth of the control group, DMSO- and 0.4 μM-5-FU-exposed spheroids, growth followed by dissociation for 4 μM 5-FU exposure and growth inhibition followed by dissociation for 40 μM 5-FU exposure—are supported by both optical assessments of the spheroid cross sections in Figure 5B and ATP assays in Figure 5C. In contrast to optical assessments and ATP assays, EIS offers the ability to monitor spheroid growth in situ in a continuous, noninvasive, and automated fashion.

Monitoring of Beating of Cardiac Microtissues

The analysis of beating human cardiac spheroids has been performed to demonstrate the ability of assessing different tissue types while using the same method and platform. The in situ assessment of cardiac beating is a particularly important feature of the platform here, as minor variations in environmental conditions—such as slight temperature changes upon transfer of the spheroids from an incubator to a microscope for optical assessment—can significantly influence the beating rate.[8] Monitoring the continuous beating of cardiac spheroids is a common readout not only to monitor cardiotoxicity effects, which usually entail a complete stop of cardiac beating, but also to detected different patterns of arrhythmia induced by proarrhythmic drugs.[20,21] Such analysis is not trivial to facilitate by optical means, as it requires in situ parallel and long-term microscopic video analysis. The system enables measurement of up to 15 spheroids in parallel. Typical yields for 4 day recordings were approximately 70%. The most common reasons for problems with spheroid measurements included evaporation and bubble formation, which entailed that tissues got stuck at a bubble inside the main channel.

Since the cardiac spheroids do not change in size, they are not studied while passing the electrodes. In order to extract their beating rates, they have to be transitionally immobilized in between the EIS electrodes. This was facilitated by moving the electrodes laterally to one end of the microchannel so that the retaining pillars are located between the electrodes (compare insets in Figure 6A to those of Figure 1D). Upon tilting the device up on the right side (t = 1 s in Figure 6A), the spheroid moves away from the retention pillars and out of the EIS sensing area. The interelectrode impedance is reduced and the output current increased. Upon tilting the device down at the right side (t = 10 s in Figure 6A), the spheroid moves back into the sensing area, and the beating of the spheroid can be detected as ripples in the baseline current. A detailed view of the beating patterns, depicted in Figure 6B, shows that the contraction of the cardiac spheroid is significantly faster than the relaxation, which is in agreement with previous observations on such cardiac spheroids.[8] An 18 h recording of the beating rate of a spheroid shown in Figure 6C revealed a regular beating of the spheroid, initially at a rate around approximately 1.1 Hz, with standard deviations as low as 0.05 Hz and a slow change of the beating rate. These results demonstrate the sensitivity of the EIS spheroid analysis method.

Conclusion

The presented platform provides an automated method to perform EIS measurements of multiple microtissue spheroids in parallel over several days. Compared to existing spheroid EIS platforms,[9–11] our system provides the following key advantages: (i) integration of EIS functions into a microfluidic spheroid device, which allows for medium perfusion and exchange, (ii) automated measurements and culturing of multiple spheroids over several days without the need to relocate the spheroids, (iii) no need for surface coating of the microfluidic device to avoid spheroid adhesion, as there is continuous tilting and spheroid movement, and (iv) continuous and independent multiparameter measurements and analysis of different spheroids and medium properties in parallel and via the same set of electrodes.

The platform enabled the automated investigation of organspecific readout parameters at suitable temporal resolution: Examples included cardiac beating and growth of cancer with and without drug dosage. The presented platform includes a pump-free setup without complex fluidic or electrical interfacing, which entails a reduced risk of contamination. The remaining manual steps in the EIS measurements of spheroids consist of spheroid and medium loading as well as medium exchanges. A future version of the device conforming with standard microtiter plate well arrangements may include automated a liquid handling system to perform these steps. An up-scaled version of this prototype platform could host multiple microfluidic chip units, which would increase throughput via parallelization while still allowing for application- or organspecific customization of the microfluidic units. The continuous EIS readout can be used to complement existing well-platebased body-on-a-chip systems for in situ drug efficacy and cardiotoxicity assessments in the same microenvironment.[22–24] In summary, the AMEIS platform constitutes a scalable technology for parallelized EIS recordings of multiple spheroids.

Supplementary Material

Refer to Web version on PubMed Central for supplementary material.

Acknowledgments

This work was supported by the European Union FP7 Grant under the project “Body on a chip” ICT-FET-296257 and an individual Ambizione Grant 142440 of the Swiss National Science Foundation for O.F. We would like to thank InSphero AG, Schlieren, Switzerland, for providing the pancreatic microislets, cardiac spheroids, and related media used in this study.

References

(1). Abbott A. Nature. 2003; 424:870–2. [PubMed: 12931155]
(2). Kelm JM, Fussenegger M. Trends Biotechnol. 2004; 22:195–202. [PubMed: 15038925]
(3). Santini MT, Rainaldi G, Indovina PL. Int J Radiat Biol. 1999; 75:787–799. [PubMed: 10489890]
(4). Pampaloni F, Reynaud EG, Stelzer EHK. Nat Rev Mol Cell Biol. 2007; 8:839–845. [PubMed: 17684528]
(5). Williamson A, Singh S, Fernekorn U, Schober A. Lab Chip. 2013; 13:3471. [PubMed: 23685915]
(6). Huh D, Torisawa Y, Hamilton GA, Kim HJ, Ingber DE. Lab Chip. 2012; 12:2156. [PubMed: 22555377]
(7). Zhang YS, Khademhosseini A. Nanomedicine. 2015; 10:685–688. [PubMed: 25816872]
(8). Beauchamp P, Moritz W, Kelm JM, Ullrich ND, Agarkova I, Anson BD, Suter TM, Zuppinger C. Tissue Eng, Part C. 2015; 21:852–861.
(9). Thielecke H, Mack A, Robitzki A. Biosens Bioelectron. 2001; 16:261–269. [PubMed: 11390213]
(10). Kloss D, Kurz R, Jahnke H-G, Fischer M, Rothermel A, Anderegg U, Simon JC, Robitzki AA. Biosens Bioelectron. 2008; 23:1473–80. [PubMed: 18289841]
(11). Luongo K, Holton A, Kaushik A, Spence P, Ng B, Deschenes R, Sundaram S, Bhansali S. Biomicrofluidics. 2013; 7
(12). Haandbæk N, With O, Bürgel SC, Heer F, Hierlemann A. Lab Chip. 2014; 14:3313–3324. [PubMed: 24984254]
(13). Gawad S, Schild L, Renaud PH. Lab Chip. 2001; 1:76–82. [PubMed: 15100895]
(14). Zhu Z, Frey O, Ottoz DS, Rudolf F, Hierlemann A. Lab Chip. 2012; 12:906–15. [PubMed: 22193373]

(15). Holmes D, Pettigrew D, Reccius CH, Gwyer JD, van Berkel C, Holloway J, Davies DE, Morgan H. Lab Chip. 2009; 9:2881–9. [PubMed: 19789739]

(16). Sukhorukov VL, Mussauer H, Zimmermann UJ. Membr Biol. 1998; 163:235–45.

(17). Gawad S, Cheung K, Seger U, Bertsch A, Renaud P. Lab Chip. 2004; 4:241–51. [PubMed: 15159786]

(18). Bürgel SC, Escobedo C, Haandbæk N, Hierlemann A. SensActuators, B. 2015; 210:82–90.

(19). Poenick S, Jahnke H-G, Eichler M, Frost S, Lilie H, Robitzki AA. Biosens Bioelectron. 2014; 53:370–6. [PubMed: 24184957]

(20). Jahnke H-G, Steel D, Fleischer S, Seidel D, Kurz R, Vinz S, Dahlenborg K, Sartipy P, Robitzki AA. PLoS One. 2013; 8:e68971. [PubMed: 23861955]

(21). Abassi YA, Xi B, Li N, Ouyang W, Seiler A, Watzele M, Kettenhofen R, Bohlen H, Ehlich A, Kolossov E, Wang X, et al. Br J Pharmacol. 2012; 165:1424–41. [PubMed: 21838757]

(22). Kim J-Y, Fluri DA, Kelm JM, Hierlemann A, Frey OJ. Lab Autom. 2015; 20:274–282.

(23). Kim J-Y, Fluri DA, Marchan R, Boonen K, Mohanty S, Singh P, Hammad S, Landuyt B, Hengstler JG, Kelm JM, Hierlemann A, et al. J Biotechnol. 2015; 205:24–35. [PubMed: 25592049]

(24). Rismani Yazdi S, Shadmani A, Bürgel SC, Misun PM, Hierlemann A, Frey O. Lab Chip. 2015; 15:4138. [PubMed: 26401602]

Europe PMC Funders Author Manuscripts

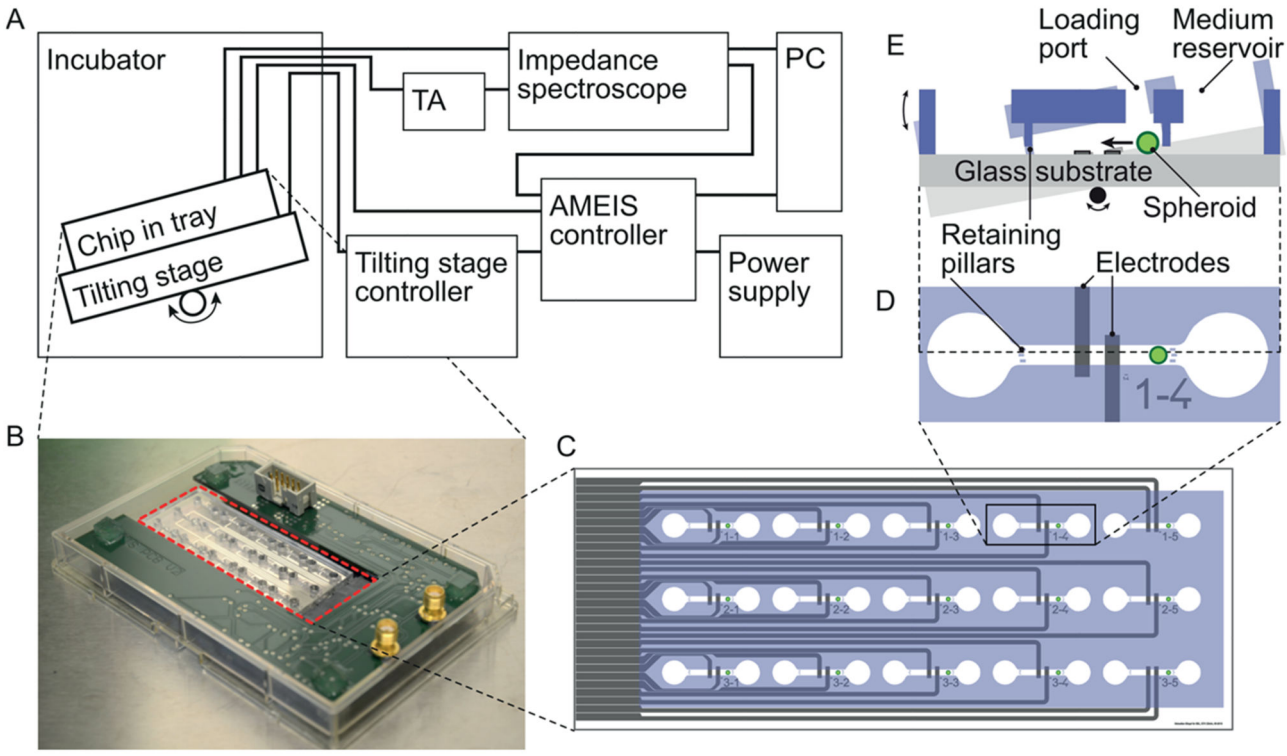

Figure 1. Overview of the AMEIS platform

(A) schematics of the entire system (TA, transimpedance amplifier); (B) chip (highlighted in dashed red line) and switch board placed in omni-tray; (C) schematic of the chip with 15 separate chambers featuring gray electrodes and blue PDMS structures; (D) close-up of one chamber with reservoirs on the left and right. The spheroid movement in the central channel (580 μm × 700 μm cross section) was confined by retaining pillars on both sides of the channel, and the coplanar EIS electrode set was arranged centrally in the channel; (E) schematic side view showing the medium reservoir and spheroid loading port, as well as the tilting-induced motion of the spheroid over the electrodes.

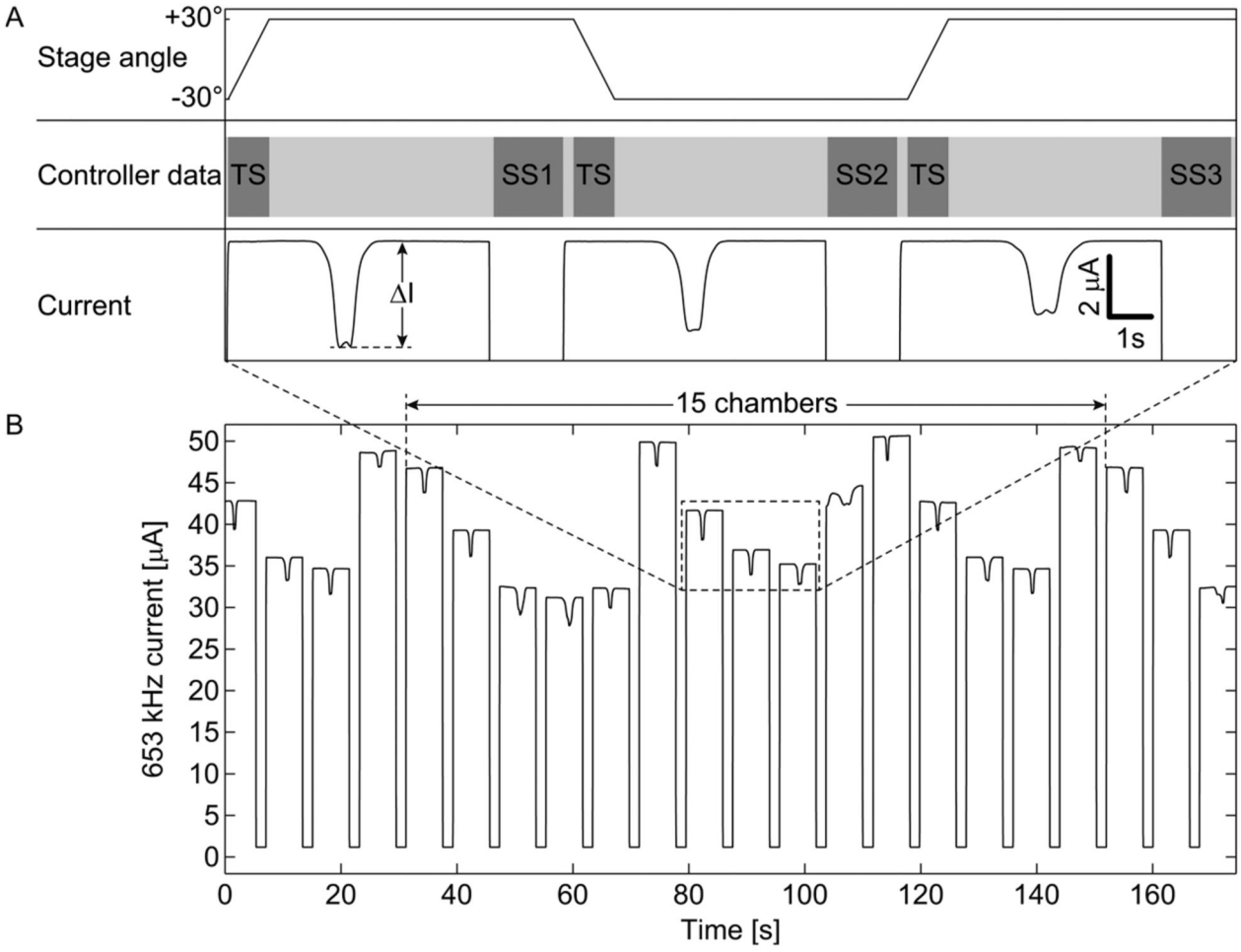

Figure 2. Measurement principle in the time domain.

(A) Temporal sequence of stage tilting, controller signals (switching sequences, indicated as SS, and tilting sequence, indicated as TS) and corresponding current dips caused by spheroids moving over the electrodes. (B) Raw current signals of an entire measurement cycle of all 15 chambers measured at 653 kHz. Δ*I* denotes peak-to-baseline signal heights.

Europe PMC Funders Author Manuscripts

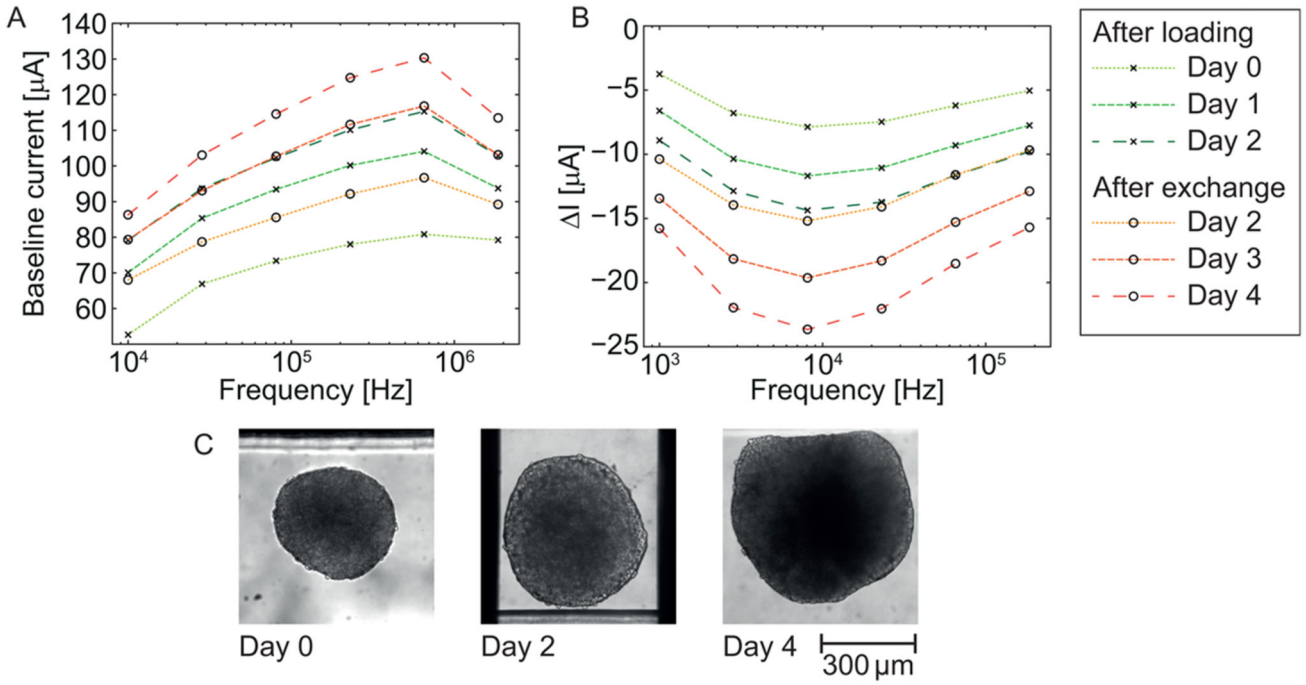

Figure 3. Current spectra of a cancer spheroid at selected time points

(A) baseline current spectra; (B) Δ*I* peak-to-baseline spectra. Spectra are shown for selected time points between days 0 and 4; on day 2, the medium in all reservoirs was exchanged so that data before and after medium exchange on the same day are shown. (C) Optical monitoring of the growth of the very same spheroid measured by EIS in panel B.

Europe PMC Funders Author Manuscripts

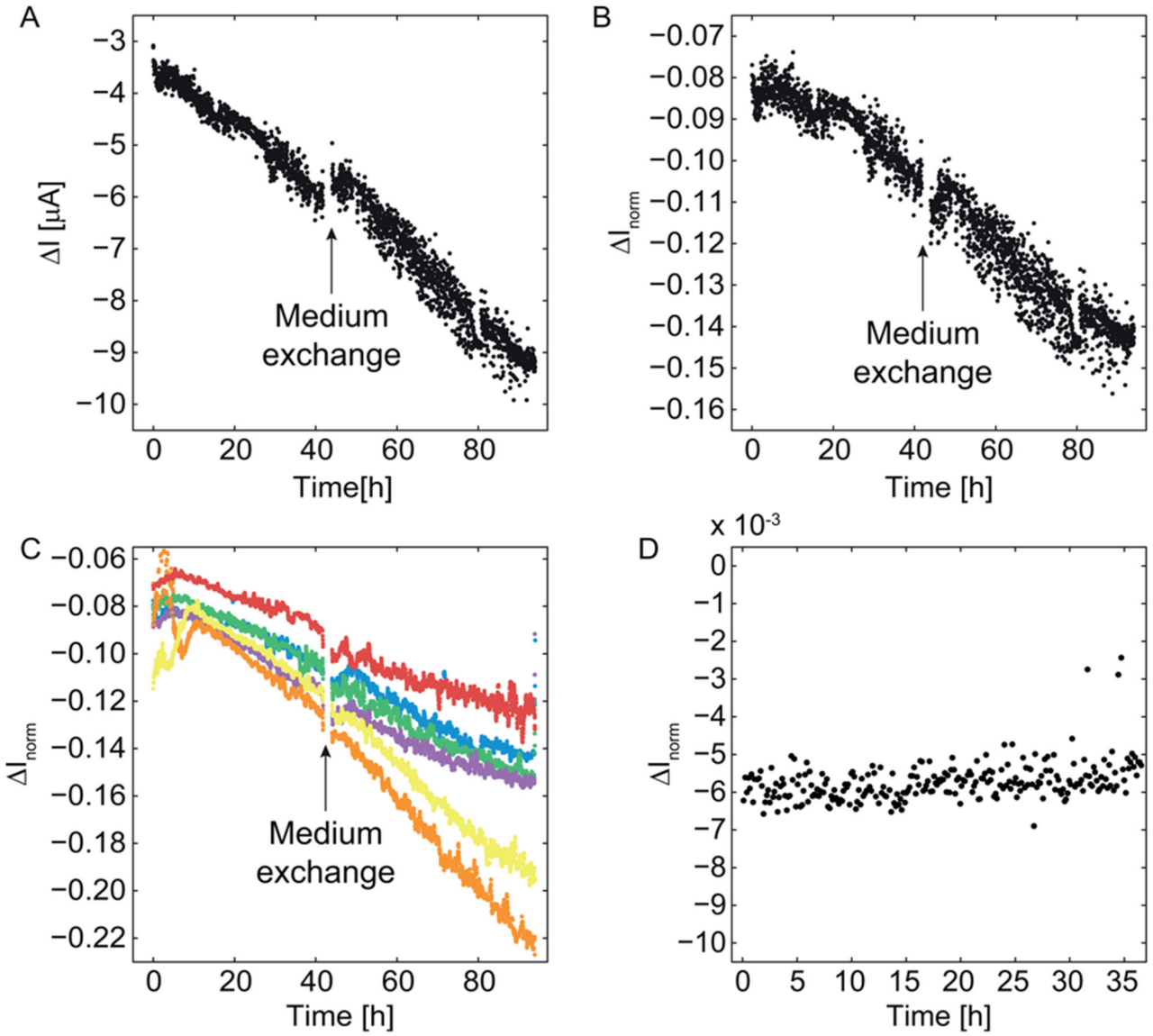

Figure 4.

Current vs time curves for growing cancer spheroids (A-C) and a pancreatic microislet, which was not expected to grow (D). (A) Continuous recordings during 90 h show a noticeable discontinuity upon medium exchange after 42 h in the peak-to-baseline (ΔI) current at 81 kHz. (B) The same data have been normalized with the corresponding baseline currents so that a growth curve without discontinuity upon medium exchange results. (C) Normalized ΔI_{norm} currents of six exemplary cancer spheroids after applying a movingaverage method including 10 subsequent measurement values. (D) ΔI_{norm} for a pancreatic microislet, which expectedly does not grow. In contrast to the cancer spheroids, there are no large variations or a current decrease. The significantly smaller values in panel D compared to panel C are a consequence of the smaller size of the microislet (150 μm diameter).

Europe PMC Funders Author Manuscripts

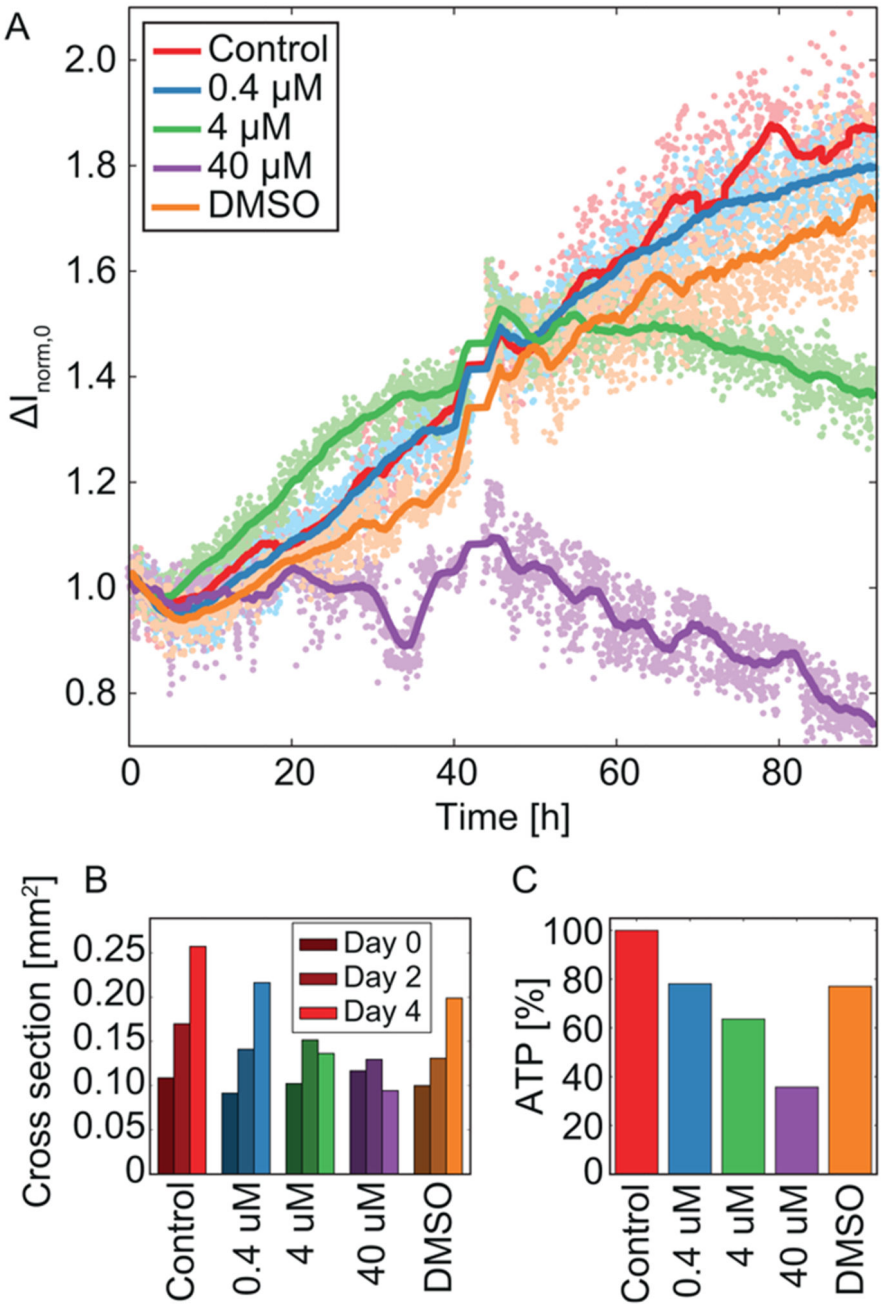

Figure 5. Impact of the drug 5-FU on HCT116 cancer spheroids.

(A) The start-point-normalized current $\Delta I_{\text{norm},0}$ of cancer spheroids which were grown in 0.4, 4, and 40 μM 5-FU, a control condition without drug, and a second control condition with just DMSO in the same concentration as has been used for the 40 μM concentration of 5-FU. The medium was exchanged after 42 h. (B) Cross section assessed via microscopy every 2 days. (C) Control-normalized ATP values at the end of the experiment. EIS data, optical size, and ATP were measured on the same tissues, respectively.

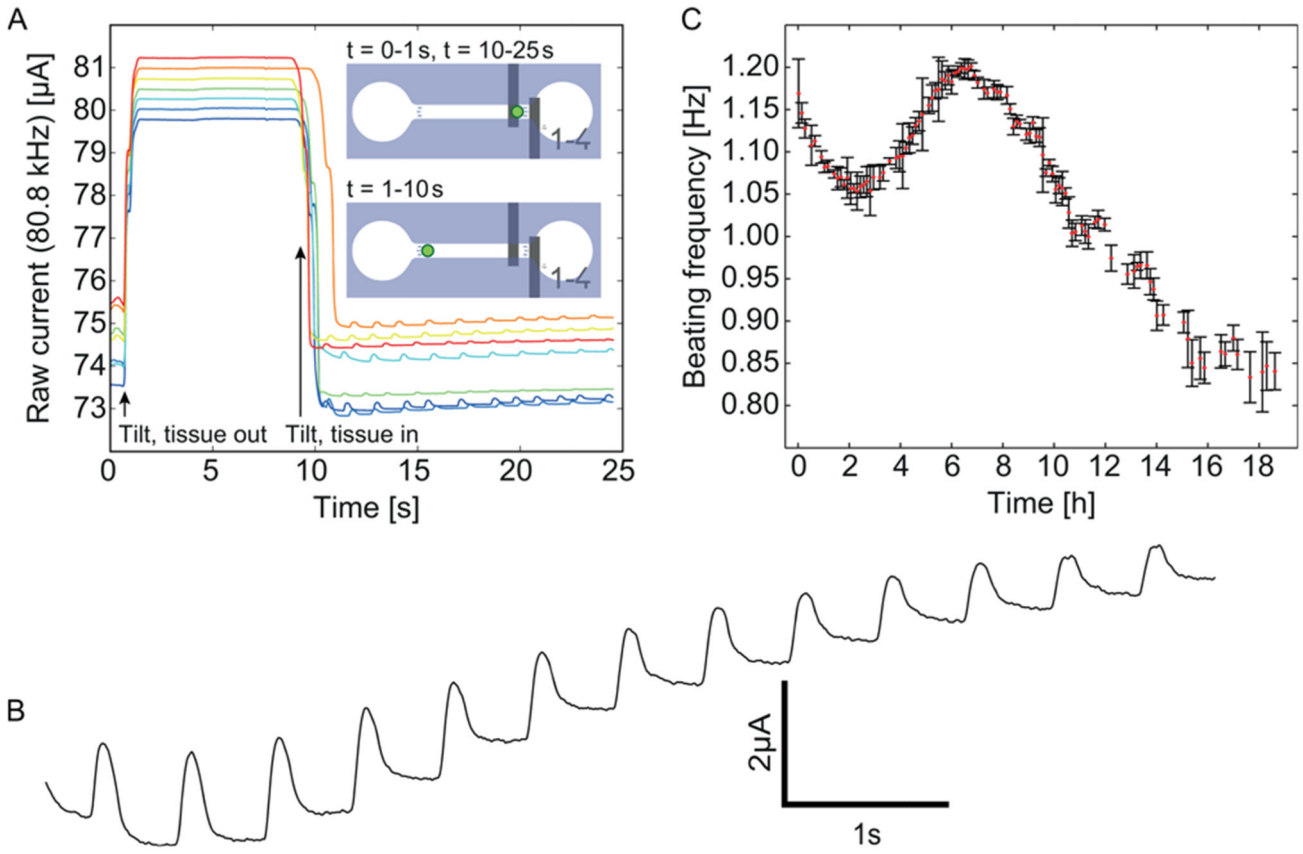

Figure 6. Measurements of cardiac spheroids.

(A) Tilting the chip with an off-center electrode arrangement allows for analysis of the cardiac beating. (B) Detailed view of a typical beating pattern when the spheroid is located between the electrodes. (C) An 18 h recording of the beating rate of a single spheroid; at each measurement point the mean beating rate and standard deviation are shown for a recording time span of 15 s (t = 10-25 s in panel A).

Europe PMC Funders Author Manuscripts